ornl

ORNL/TM 13515

OAK RIDGE
NATIONAL
LABORATORY

LOCKHEED MARTIN

Application of Polynomial and Radial Basis Function Maps To Signal Masking

B. Damiano
J. E. Breeding

MANAGED AND OPERATED BY
LOCKHEED MARTIN ENERGY RESEARCH CORPORATION
FOR THE UNITED STATES
DEPARTMENT OF ENERGY

ORNL/TM-13515

APPLICATION OF POLYNOMIAL AND RADIAL BASIS FUNCTION MAPS TO SIGNAL MASKING

B. Damiano
J. E. Breeding
Instrumentation and Controls Division

Date Published—January 1998

Research sponsored by the Laboratory Directed Research Program of Oak Ridge National Laboratory.

Prepared by
Oak Ridge National Laboratory
Oak Ridge, Tennessee 37831-6285
Managed by
LOCKHEED MARTIN ENERGY RESEARCH CORP.
for the
U.S. DEPARTMENT OF ENERGY
under contract number DE-AC05-96OR22424

CONTENTS

LIST OF FIGURES

ACRONYMS

LPE/LPI - low probability of exploitation/intercept

RBF - radial basis function

SSN - submarine

SWMCM - shallow water mine-counter-mine

USNS - United States Navy Ship

UUV - unmanned underwater vehicle

ABSTRACT

The objective of this research was to develop and demonstrate a technique for encrypting information by using a masking signal that closely approximates local ambient noise. Signal masking techniques developed to date have used nonlinear differential equations, spread spectrum, and various modulation schemes to encode information. While these techniques can effectively hide a signal, the resulting masks may not appear as ambient noise to an observer. The advantage of the proposed technique over commonly used masking methods is that the transmitted signal will appear as normal background noise, thus greatly reducing the probability of detection and exploitation. A promising near-term application of this technology presents itself in the area of clandestine minefield reconnaissance in shallow water areas. Shallow water mine-counter-mine (SWMCM) activity is essential for minefield avoidance, efficient minefield clearance, and effective selection of transit lanes within minefields. A key technology area for SWMCM is the development of special sonar waveforms with low probability of exploitation/intercept (LPE/LPI) attributes. In addition to LPE/LPI sonar, this technology has the potential to enable significant improvements in underwater acoustic communications. For SWMCM, the chaotic waveform research provides a mechanism for encrypted communications between a submarine (SSN) and an unmanned underwater vehicle (UUV) via an acoustic channel. Acoustic SSN/UUV communications would eliminate the need for a fiberoptic link between the two vessels, thus increasing the robustness of SWMCM. Similar applications may exist in the areas of radar masking and secure communications.

The original approach called for the use of polynomial maps to generate a masking signal. Because polynomial maps were found to have highly restrictive stability criteria, our approach was modified to use radial basis function (RBF) maps. We have shown that stable RBF maps that closely approximate an ambient sea state can be derived using nonlinear systems theory. In doing so, we have shown that our measured ambient state has a deterministic structure that implies eight-order dynamics. The RBF maps were used to successfully encrypt a continuous wave signal across a high-fidelity, low-noise transmission path. Attempts to duplicate this result across a low-fidelity, high-noise path were not successful.

1. INTRODUCTION

The objective of this research was to develop and demonstrate a technique for masking information, which may be in the form of a sonar pulse or a communications signal, by using a signal that closely approximates local ambient noise. Signal masking techniques developed to date have used nonlinear differential equations, spread spectrum, and various modulation schemes to encode information. While these techniques can effectively hide a signal, the resulting masks may not appear as ambient noise to an observer. The advantage of the investigated technique over commonly used masking methods is that the transmitted signal appears as normal background noise, thus greatly reducing the probability of detection and exploitation.

The investigated technique uses a map obtained by applying nonlinear systems theory to relate the state vector describing the ambient noise at time t_0 to the state vector at time $t_0 + \delta t$. The resulting map is used to generate a masking signal, which is then modulated with the information signal before being transmitted. The received signal is demodulated by using a priori knowledge of the masking signal.

1.2 TECHNICAL BACKGROUND

The effectiveness of the encryption depends heavily on the generation of an appropriate masking signal. Ideally, the masking signal will closely simulate background noise while remaining easy to demodulate. This section describes approaches employing nonlinear systems theory to generate masking signals that accomplish one or the other of these goals.

1.2.1 Masking Signal Simulating Ambient Noise by Using a Chaotic Time Series

Recent work suggests that many commonly encountered forms of ambient noise may be closely described by a deterministic model with chaotic behavior, and that expansions in polynomials or other functions can be used to obtain a model of the dynamics for such noise.[1,2,3,4] This model can be used to generate a deterministic masking signal closely approximating the ambient noise.

Assuming that the ambient noise can be described by a deterministic model, a relationship, G, describing the dynamics of the noise must exist,

$$X(t) = G[X(t_0)] \ , \tag{1}$$

where X is a d-dimensional vector of phase space variables describing the noise, t is time, and t_0 is some initial time. In the practical cases we will consider, a single observable variable Y of the system is measured at equally spaced time intervals, Δt, where Y is some unknown function of the state variables, X [e.g., $Y = H(X)$]. For such a time series, the ith measurement is given by

$$Y_i = H[\, X(i\Delta t)\,] \ . \tag{2}$$

The following conditions will be assumed to be satisfied by the scaler time series Y and by the dynamics of the system:

- The time series consists of measurements obtained at equally spaced time increments.
- The time series sampling satisfies the Nyquist sampling criteria.
- The dynamics are such that for initial conditions within some region of phase space, all trajectories converge toward a common asymptotic solution, A. This asymptotic solution is called an attractor because all initial conditions within the region are attracted to this solution.
- The time series is obtained after any transient portion of the solution has, for all practical purposes, died away. Thus, the time series describes the dynamics of the attractor A, and our attention can be limited to the dynamics of A.
- The attractor is ergodic and the time series captures a representative sample of the dynamics of A.

Because G, H, and d are unknown, the original attractor cannot be recovered. However, it is possible to construct representative state vectors in an appropriate embedding phase space from the scaler time series and use these state vectors to form a reconstructed attractor. The trajectories in such an embedding are found to faithfully reproduce the invariant dynamical features of the original system, G.

The method of delays, being the simplest method for constructing state vectors in an embedded phase space, was used in this work. The form of the kth state vector, $\boldsymbol{Z}^{\boldsymbol{k}}$, is given by

$$\boldsymbol{Z}^{\boldsymbol{k}} = [Y_k, Y_{k+\mathrm{T}}, Y_{k+2\mathrm{T}}, \ldots . Y_{k+(d_e-1)\mathrm{T}}] , \tag{3}$$

where T is the delay increment, $Y_{k+\mathrm{T}} \ldots Y_{k+(de-1)\mathrm{T}}$ are the embedded variables, and d_e is the embedding dimension.[5] The state vectors constructed by using the method of delays obviously depend on the embedding dimension and the delay increment.

Taken's theorem states that for an infinite noise-free time series, an embedding exists such that the invariant features of the reconstructed dynamics will be the same as those of the original system.[6] Moreover, an embedding dimension of no greater than $2d + 1$ will be sufficient to preserve these invariant features. Under realistic conditions, where the time series contains a finite number of data points contaminated by noise, it is found that the dynamics in the embedded phase space depend on both the embedding dimension and the delay increment. Thus, the dynamics of the reconstructed attractor will approach those of the original attractor only for a proper choice of d_e and T.

Returning to the problem of modeling ambient noise by using a polynomial map, we propose to find a map $\boldsymbol{F}$ that relates the reconstructed observables at time increment n to those at time increment n+1:

$$\boldsymbol{Y}^{n+1} = \boldsymbol{F}(\boldsymbol{Y}^n) \ . \tag{4}$$

The components of the $\boldsymbol{F}$ can be represented by a set of polynomials $P_j(\boldsymbol{Y})$ expanded up to order p:

$$F_i(\boldsymbol{Y}) = \sum_{k=1}^{p} C_{i,k} P_k(\boldsymbol{Y}) \ , \tag{5}$$

where the $P_j(\boldsymbol{Y})$ are constructed to be orthonormal on the data set; that is,

$$\sum_i P_k(\boldsymbol{Y}_i) P_l(\boldsymbol{Y}_i) = \delta_{kl} \ . \tag{6}$$

The polynomial construction consists of forming polynomial maps $\boldsymbol{F}$ as a function of the embedding dimension and the delay increment. The coefficients $C_{i,k}$, along with the optimum values of d_e and T, may be determined by minimizing the error $E(C_{i,k})$, which is given by

$$E(C_{i,k}) = \sum_n \sum_i [\, Y_i^{n+1} - F_i(\boldsymbol{Y}^n)]^2 = \sum_n \sum_i [\, Y_i^{n+1} - \sum_{k=1}^{p} C_{i,k} P_k(\boldsymbol{Y}^n)]^2 . \tag{7}$$

A synthetic time series closely resembling the ambient noise in both the time and frequency domain can be generated from $\boldsymbol{F}$. This synthetic time series will be used as our masking or carrier signal.

1.3 RESEARCH OVERVIEW

The objective of this research was to develop and demonstrate a technique for encrypting information by using masking signals that closely approximate local ambient noise. The masking signals will be generated by using either polynomial or radial basis function (RBF) maps. The main steps performed during the research were as follows:

- Develop a systematic method to calculate the map coefficients for polynomial maps and RBF maps. The resulting maps must be stable in the sense that they do not converge to either a fixed point or a limit cycle under iteration, and the iterated map must closely approximate the background signal in both the time and frequency domains.

- Develop a method to synchronize the decrypting map at the receiver with the encrypting map at the transmitter.

- Develop a method to take the effects of the transmission path into account when performing decryption.

- Demonstrate the method using both simulated signals and measured noise (i.e., background) signals.

The remainder of the report describes the investigation and its results. Section 2 describes map generation for both polynomial and RBF maps and presents some sample maps approximating synthetic time series. Section 3 presents the results of applying the map generation method described in Sect. 2 to measured noise data. Section 4 describes signal masking and recovery and how the problem of synchronization was overcome. Section 5 presents signal recovery results using maps created by using both synthetic and measured masking signals. The final section presents conclusions based on the investigation and discusses the investigation results The report concludes with a discussion of further research needed to extend the investigation results toward the goal of creating a practical masking/recovery system based on the investigated method.

2. MAP CREATION METHODOLOGY

A key aspect of this work was to develop a methodology to create maps that approximate the dynamic behavior of measured time series. These maps would be used to generate a masking signal used at both the transmitter and receiver. These maps need to closely approximate the dynamics of the measured time series to reduce the probability of signal detection and exploitation.

An acceptable map must perform two functions well. First, it must be a good one-step predictor; that is, given some number of previous measurements, it must be able to predict the value of the next measurement. Second, under iteration, the map must closely approximate the dynamics of the measured time series. The first requirement, that the map must be a good one-step predictor, is used during demodulation of the received signal. The second requirement, that the map must approximate the system dynamics under iteration, is needed to create the masking signal at the transmitter.

Nonlinear time series analysis techniques have been applied to characterize the measured time series and determine some key parameters needed for map creation. These key parameters were used to create both polynomial maps and maps composed of RBFs. The ability of these maps to perform as one-step predictors and to simulate system dynamics under iteration were investigated. This section describes the application of nonlinear time series analysis methods, the calculation of the polynomial and RBF maps, and the performance of the resulting maps. Sample results using time series obtained from the Lorenz system of nonlinear differential equations are used to demonstrate the calculations.

2.1 APPLICATION OF NONLINEAR TIME SERIES ANALYSIS TECHNIQUES

Nonlinear time series analysis techniques are used to examine whether the measured time series is deterministic, to ascertain the optimum time delay used to reconstruct the attractor, and to determine the minimum embedding dimension of the reconstruction. If the measured time series is entirely random, any attempt to create a map to approximate and predict the measured time series will be futile. For deterministic systems, the underlying dynamics can be characterized from a time series by applying the method of delays.[5] The dynamics will usually be multidimensional, with the dimension being initially unknown. Once the multidimensional attractor is reconstructed from the measured time series, a map that approximates this attractor can be created.

The mutual information function is used to determine whether the measured time series is deterministic and, if so, to determine the time delay to use in reconstructing the attractor. The method of global false nearest neighbors is used to determine the embedding dimension of the reconstructed attractor. The following sections describe these two methods.

2.1.1 Mutual Information

It is generally accepted that the optimum time delay, τ, used to reconstruct an attractor from a time series corresponds to the time at which the first minimum occurs in the mutual information function.[7] The time delay corresponding to the first minimum in the mutual information function is the minimum time interval necessary for two variables to become essentially uncorrelated. An attractor reconstructed by using τ as the delay time will have uncorrelated components while avoiding the "folding" typical of using values of time delay that are too large.

The mutual information function is similar to the autocorrelation function, except that it measures the general dependence of two variables rather than only the variable's linear dependence. Note that random data will be uncorrelated; thus, the mutual information function can be used to indicate whether a time series contains correlated information from a deterministic source or whether the time series is simply random noise.

The derivation of the mutual information function for two series of measurements S and Q, $I(S,Q)$, is given in Ref. 7. The resulting expression for $I(S,Q)$ is

$$I(S,Q) = H(S) + H(Q) - H(S,Q) \ , \tag{8}$$

where H is the entropy of the series of measurements. If the series of N measurements of S is given by $(s_1, s_2, s_3, ..., s_N)$, then the entropy, $H(S)$, is given by

$$H(S) = -\sum_{i=1}^{N} P_s(s_i) \log_2 \left[P_s(s_i) \right] \ , \tag{9}$$

where $P_s(s_i)$ is the probability of a measurement being equal to s_i.

In a similar manner, if $S = (s_1, s_2, s_3, ..., s_N)$ and $Q = (q_1, q_2, q_3, ..., q_N)$ are two sets of measurements, then the entropy of the combined set of measurements, $H(S,Q)$, is given by

$$H(S,Q) = -\sum_{i=1}^{N} \sum_{j=1}^{N} P_{sq}(s_i,q_j) \log_2 \left[P_{sq}(s_i,q_j) \right] \ , \tag{10}$$

where $P_{sq}(s_i,q_j)$ is the probability of q_j occurring if s_i is known to occur. In this application, S

corresponds to the time series, and Q is obtained from S by delaying S by ΔT.

The mutual information is calculated by using Eqs. (1), (2), and (3) for a range of delay times. For a deterministic time series, plotting the values of $I(S,Q(\Delta T))$ (where the dependence of Q on the delay time is explicitly shown) against delay time results in initially decreasing values of $I(S,Q(\Delta T))$ as delay time increases. $I(S,Q(\Delta T))$ eventually will pass through a minimum and then vary, always remaining at a relatively low value. The value of delay time at which the first minimum of $I(S,Q(\Delta T))$ occurs is the reconstruction delay time, τ, selected to perform the attractor reconstruction.

2.1.2 Method of Global False Nearest Neighbors

The method of global false nearest neighbors is based on a simple geometric idea: if the number of dimensions d used to reconstruct an attractor is too small, many points that appear "near" will become widely separated when $d + 1$ dimensions are used in the attractor reconstruction.[8] Nearest neighbor points that experience this wide separation when comparing their distances in dimension d and $d + 1$ are false nearest neighbors in dimension d. Conversely, true nearest neighbors will remain near each other in attractor reconstructions of both d and $d + 1$ dimensions. The adequacy of dimension d for reconstructing an attractor can be evaluated by selecting a number of random points and their nearest neighbors in dimension d and then calculating the percentage of false nearest neighbors.

Typical results of this calculation for noise-free data show the percentage of false nearest neighbors to be relatively high for low-dimensional attractor reconstructions, with the percentage of false nearest neighbors decreasing with increasing dimension, eventually reaching and remaining at a value near zero. The lowest dimension at which the percentage of false nearest neighbors is the minimum embedding dimension needed to reconstruct the data, d_e. Noisy data show similar results, except the percentage of false nearest neighbors reaches a minimum at d_e and then increases with increasing dimension. The minimum percentage of false nearest neighbors will not approach zero for noisy data; the amount of random noise contamination will determine the value of the minimum in the global false nearest neighbors calculation results.

A pair of points are considered false nearest neighbors in dimension d if

$$\frac{R^2_{d+1}(n)}{R^2_d(n)} > R_{tol}\,, \tag{11}$$

where $R_d(n)$ is the Euclidean distance between the nth point and its nearest neighbor in d dimensions, $R_{d+1}(n)$ is the Euclidean distance between the nth point and its nearest neighbor in

$d+1$ dimensions, and R_{tol} is the first criteria for declaring nearest neighbor pairs to be false.[8] A second criteria, needed because near neighbors may not be especially "close," is given by

$$\frac{R^2_{d+1}}{\sigma^2} > A_{tol} , \tag{12}$$

where σ is the standard deviation of the time series and A_{tol} is the second criteria for declaring nearest neighbor pairs to be false.[8] A nearest neighbor pair is declared false if either test [Eqs. (4) and (5)] fails. In this work, the values used for the criteria in Eqs. (4) and (5) are $R_{tol} = 17.1$ and $A_{tol} = 1.8$.

2.1.3 The Lorenz System

The Lorenz system consists of the following nonlinear set of equations:

$$\frac{dX}{dt} = \sigma(Y - X) , \tag{13}$$

$$\frac{dY}{dt} = rX - Y - XZ , \tag{14}$$

and

$$\frac{dZ}{dt} = -bZ + XY , \tag{15}$$

where σ, r, and b are constants and X, Y, and Z are the time-dependent coordinates.[9] A thorough description of the Lorenz system and its derivation is given in Ref. 9.

Equations (13), (14), and (15) were integrated by using a fourth-order Runge Kutta numerical integration algorithm. Values of $\sigma = 10$, $r = 28$, and $b = 8/3$; initial conditions of $X = 0.01$, $Y = 0.02$, and $Z = 0.15$; and an integration step size of 0.0005 seconds were used in the calculation. Values of X, Y, and Z were tabulated for 0.005 second intervals. The Lorenz attractor is shown in Fig. 1.

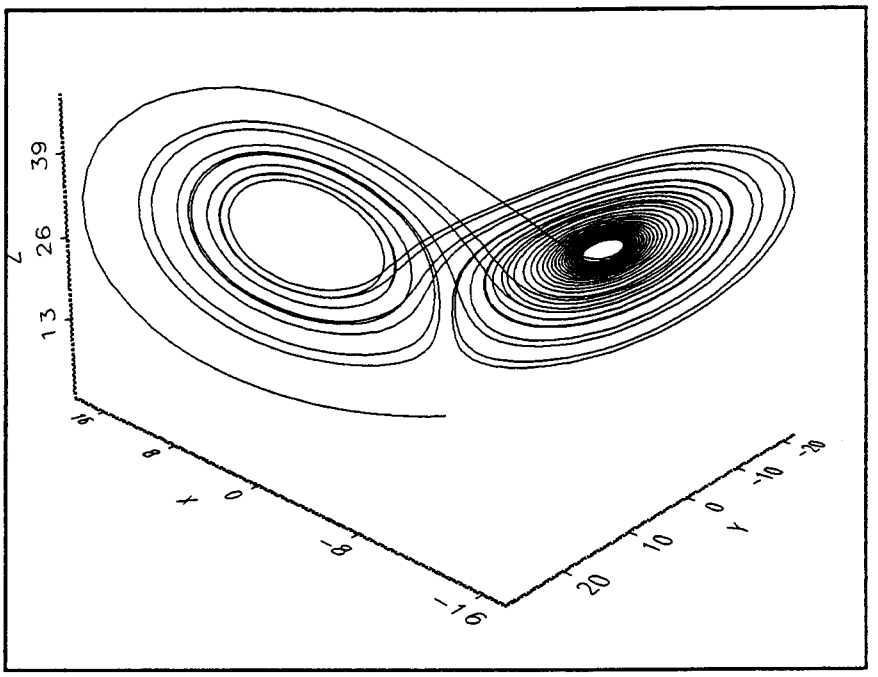

Fig. 1. The Lorenz attractor calculated for $\sigma = 10$, $r = 28$, and $b = 8/3$ using the initial conditions $X = 0.01$, $Y = 0.02$, and $Z = 0.15$.

The attractor used in the map calculation was obtained from the X coordinate by using the method of delays. The optimum time delay for the reconstruction was set equal to the first minimum in the mutual information function. Figure 2 shows the mutual information calculated from the X coordinate of the Lorenz system for a range of time delays. The optimum time delay for attractor reconstruction is 0.16 seconds. Figure 3 shows the results of the global false nearest neighbor calculation. Results show that the proper choice for d_e is three. Three dimensions were used in the attractor reconstruction; a two-dimensional representation of the reconstructed attractor is shown in Fig. 4. Thus, when attempting to create a map of the Lorenz system, an attractor reconstruction of dimension of three or greater and a time of delay of 0.16 seconds should be used.

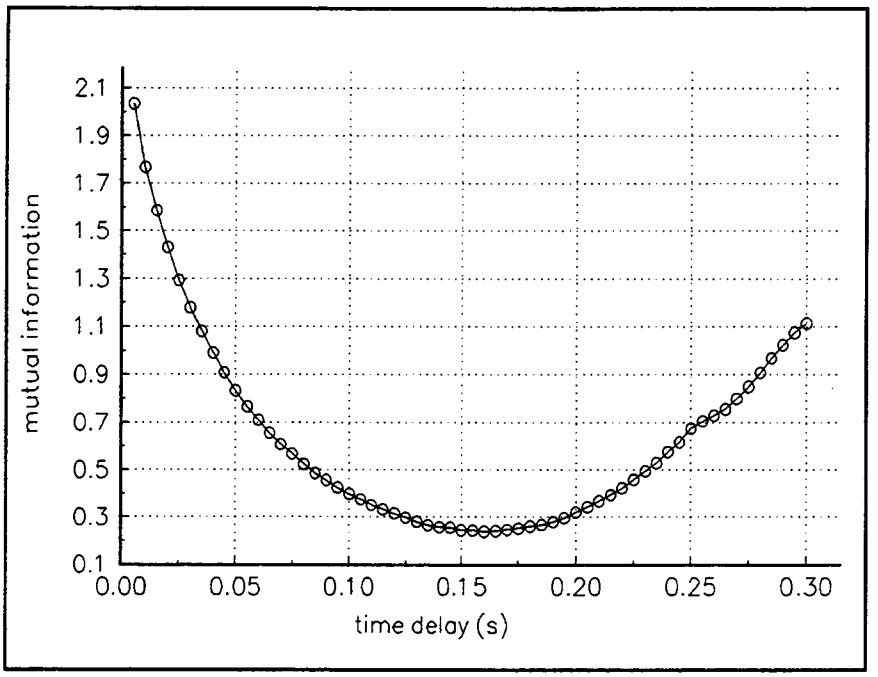

Fig. 2. Effect of time delay on the mutual information of the Lorenz system.

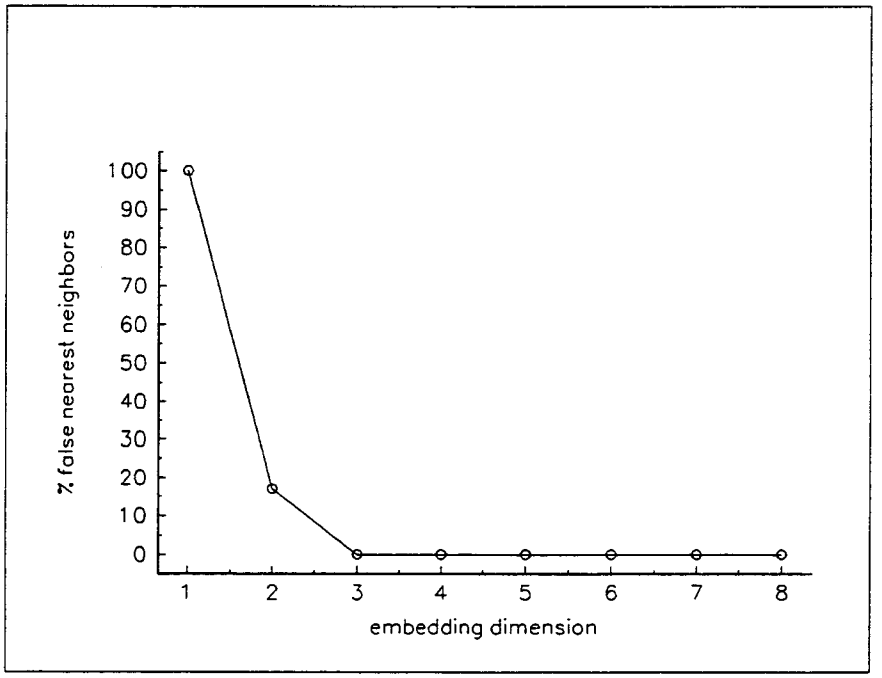

Fig. 3. Global false nearest neighbor calculation results for the Lorenz attractor ($d_e = 3$).

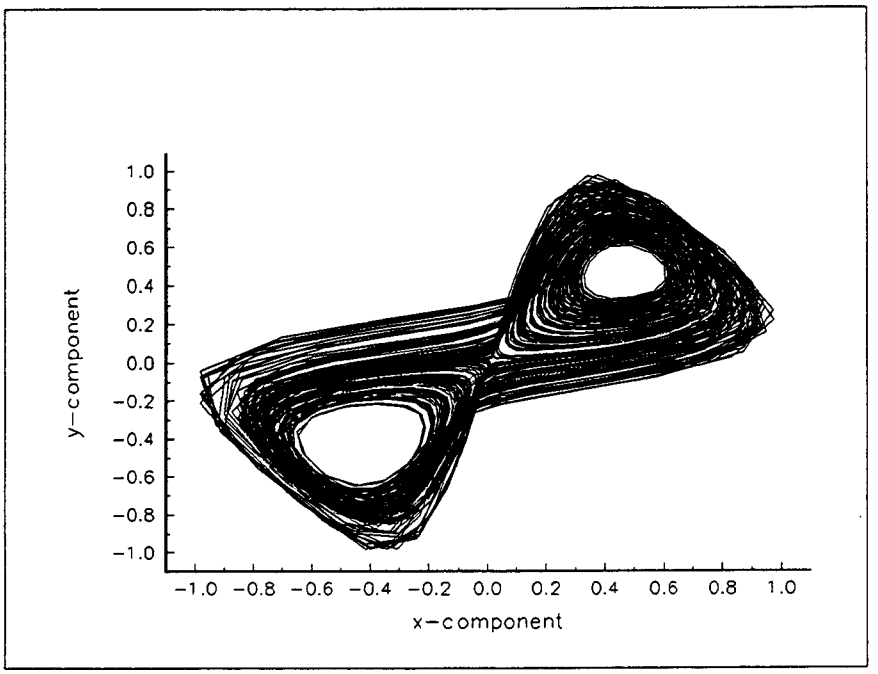

Fig. 4. The reconstructed Lorenz attractor in two dimensions.

2.2 CREATION OF MAPS COMPOSED OF POLYNOMIALS

The first attempt to create maps that simulate system dynamics under iteration involved using polynomials. Polynomials are easy to work with and are familiar, and there is considerable experience in using them to obtain one-step prediction maps, often for the purpose of calculating the Liapunov spectrum.[10] Furthermore, the successful iteration of polynomial maps to simulate system dynamics has been documented.[3,4,11] The general form of the polynomials maps used in this work is given by

$$x_{i+1} = \sum_{n=1}^{N} \lambda_n M_{n,i} \,, \tag{16}$$

where x is the time series variable, i is the ith iterate, n is the number of terms in the map, λ_n is the coefficient of the nth term, and $M_{n,i}$ is the nth monomial created from the state vector components of iterate i. As an example, for a three-dimensional system, the polynomial map would be given by

$$x_{i+1} = \lambda_0 + \lambda_1 x_i + \lambda_2 y_i + \lambda_3 z_i + \lambda_4 x_i^2 + \lambda_5 y_i^2 + \lambda_6 z_i^2 + \lambda_7 x_i y_i + \lambda_8 x_i z_i + \lambda_9 y_i z_i \,. \tag{17}$$

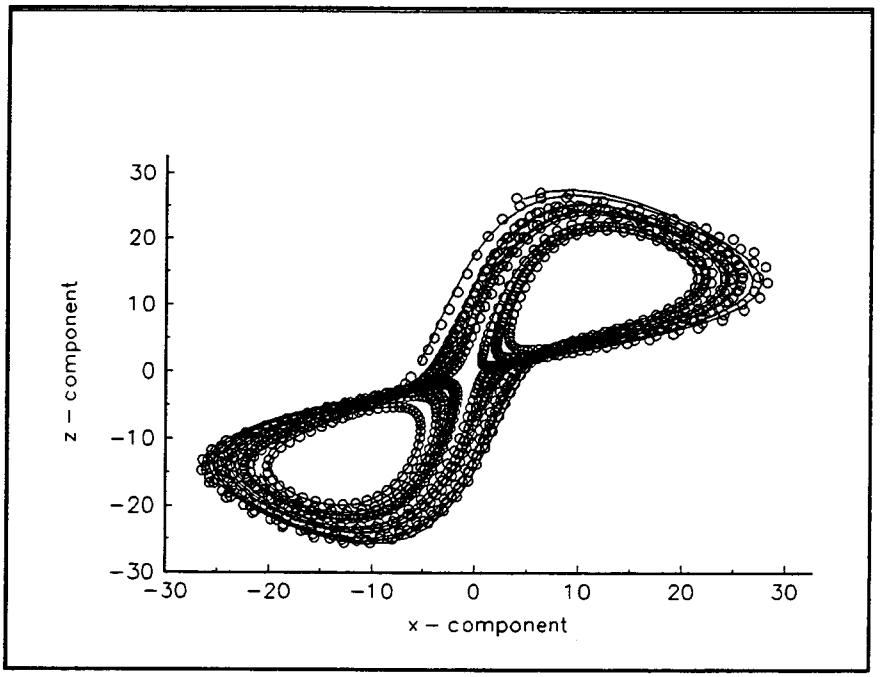

Fig. 5. The Lorenz attractor and it's image. The solid line corresponds to the original data and the circles correspond to the image.

The values of the λ_n are determined by performing a least squares fit to M data points using singular value decomposition. A good map will have an image of the data set that closely matches the data set and will reproduce the system dynamics under iteration. The following sections present results.

2.2.1 Calculation Results for Polynomial Maps

Polynomial maps were calculated for the Lorenz system. The performance of the polynomial map was evaluated by comparing the image of the data to the data, and by comparing the time series and attractors of the data and the iterated map.

Figure 5 shows a comparison of the reconstructed attractor and the image of an attractor generated by a second-order polynomial map. Five thousand data points were used to fit the map coefficients. The image of the map closely approximates the attractor. This result indicates that the polynomial map would be an accurate one-step predictor.

Figure 6 shows the attractor of the iterated map. The map rapidly approaches a fixed point under iteration. This result is typical of our findings using polynomial maps. Another common result is that polynomial maps are often unstable under iteration; that is, their iterates eventually become unbounded. It appears that it is rare (and this assertion is borne out by the discussion in

Ref. 3 to find a polynomial map that will closely approximate system dynamics under iteration. Thus, the instability of polynomial maps under iteration resulted in our abandoning them for this application in favor of RBF maps.

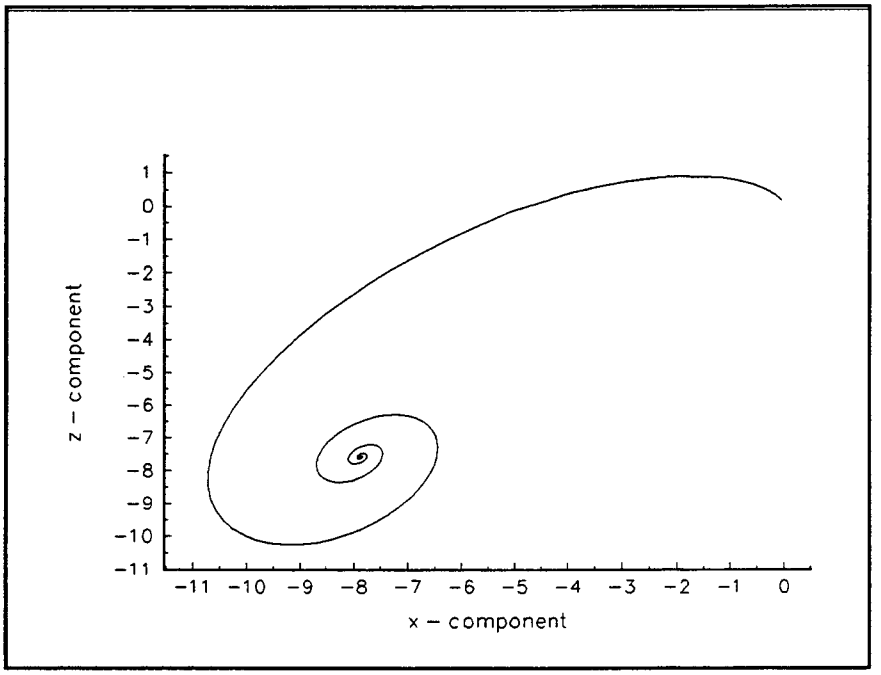

Fig. 6. The result of iterating the unconstrained polynomial map for the Lorenz attractor. This result is typical.

2.3 MAPS COMPOSED OF RADIAL BASIS FUNCTIONS

The inability to obtain polynomial maps that closely simulate system dynamics when iterated led to the investigation of maps composed of RBFs. These functions have good localization properties and normally remain bounded when iterated.

2.3.1 Description of Radial Basis Function Maps

The general form of a map composed of such functions is given by

$$x_{i+1} = \sum_{n=1}^{N} \lambda_n \phi_{n,i}(\|x_i - \alpha_n\|) \ , \tag{18}$$

where x is the time series variable, i is the ith iterate, n is the number of terms in the map, λ_n is the

coefficient (or weight) of the nth term, $\phi()$ is the RBF, and α_n is the nth basis vector.[12] Note that the Euclidean norm between the point x_i and the basis vector α_n is the argument supplied to the function $\phi()$. Following the example described in Ref. 12, the form of the RBF $\phi()$ used in this work is given by

$$\phi(r) = (r^2 + C^2)^{-\beta} , \tag{19}$$

here $\beta > -1$, $\beta \neq 0$, and C is a constant. Substituting the Euclidean norm into Eq. (19) for r yields the form for the RBF used in this work:

$$\Phi_{n,i} = \left(\sum_{k=1}^{d_e} \left(x_{i,k} - \alpha_{n,k}\right) + C^2 \right)^{-\beta} . \tag{20}$$

The values of the λ_n are determined by fitting the first n data points. This fitting results in the following equation that must be satisfied by the λ_n:

$$\{x\}_{i+1} = [\Phi]\{\lambda\} , \tag{21}$$

where $\Phi_{n,i} = \phi_{n,i}$. The λ_n are given by

$$\{\lambda\} = [\Phi]^{-1}\{x\}_{i+1} . \tag{22}$$

A computer code was written to implement the calculation of the λ_n and to iterate the resulting RBF map. The following section shows the results.

2.3.2 Calculation Results for Radial Basis Function Maps

RBF maps were calculated for the Lorenz system. The performance of the RBF maps is evaluated by comparing time series, attractors, and Fourier transforms of the original time series and the time series generated by iterating the maps.

2.3.2.1 Results for the Lorenz System

A 400-term RBF map was created using values of $\beta = 1$ and $C^2 = 0.5$ and an embedding dimension of six. The time series was scaled to be between -1 and 1. The original and simulated time series, attractors, and Fourier transforms are compared in Figs. 7 to12. Note that the original and simulated time series match virtually exactly for the first 400 data points: these points; are used as the basis vectors, so this agreement is not surprising. The original and simulated time series show good agreement for approximately the next 100 map iterations, after which the simulated time series diverges from the original time series. However, the qualitative behavior of the two time series remains similar, as shown by the close agreement between the original and simulated time series, attractors, and Fourier transforms.

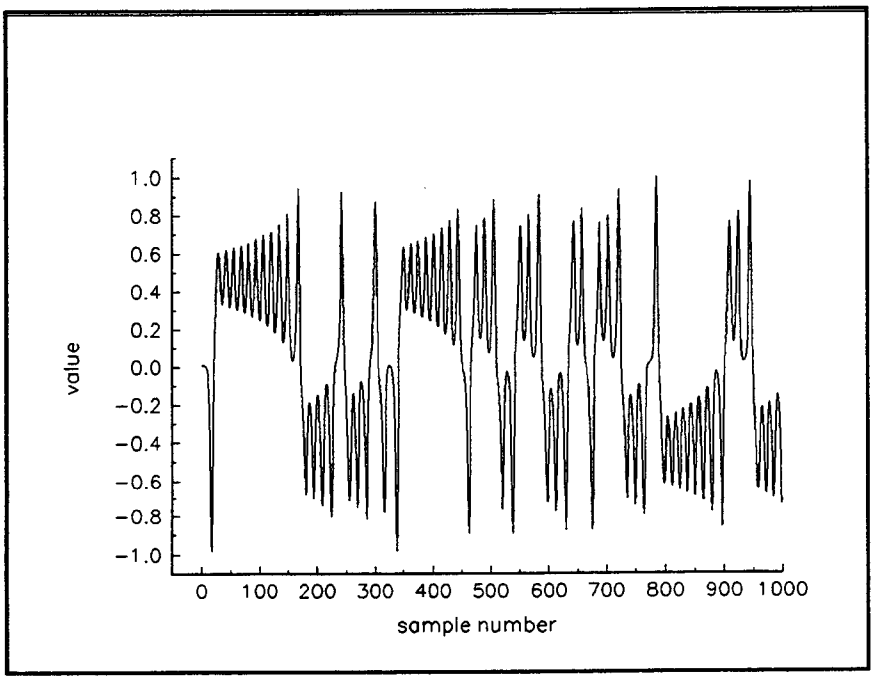

Fig. 7. The time series of the Lorenz attractor. Samples are taken every .05 seconds.

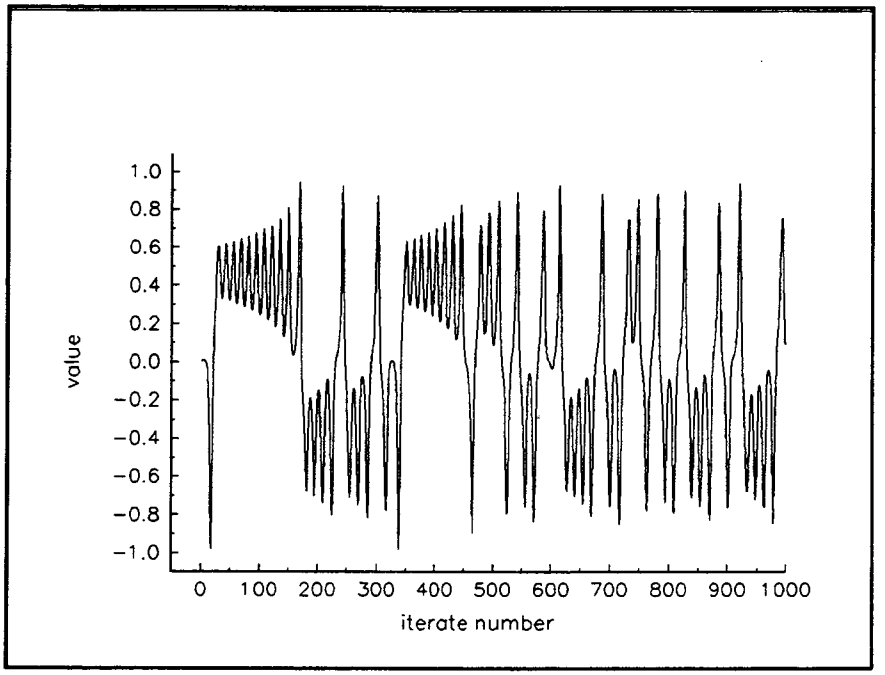

Fig. 8. The time series generated from iterating the map. The map has 400 terms and is composed of radial basis functions with $\beta = 1$ and $C^2 = 0.5$. Six dimensions are used in the reconstruction with a time delay of 0.15 seconds.

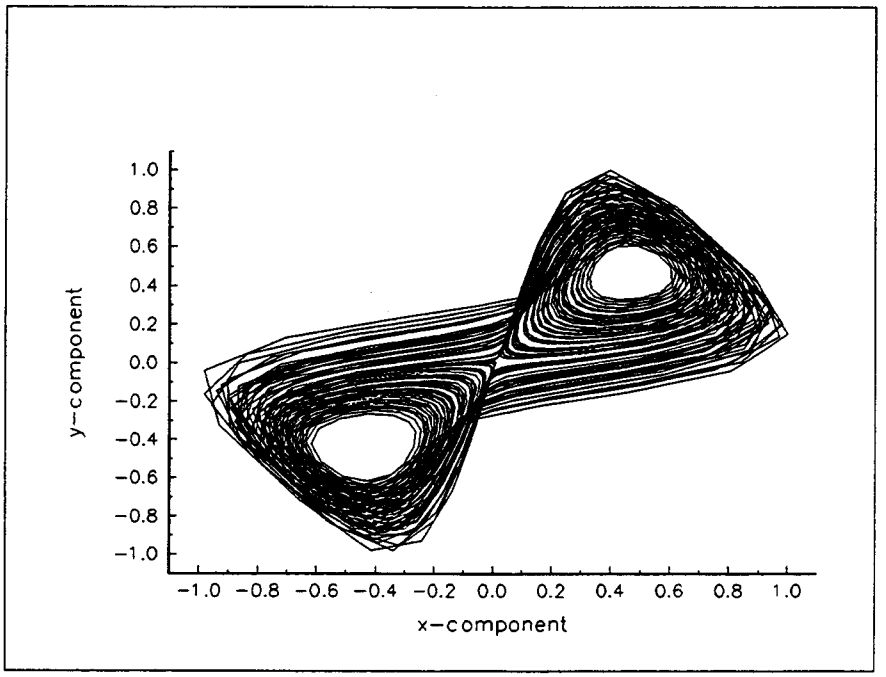

Fig. 9. The attractor reconstructed by using delay coordinates for the Lorenz system. Three thousand points are shown.

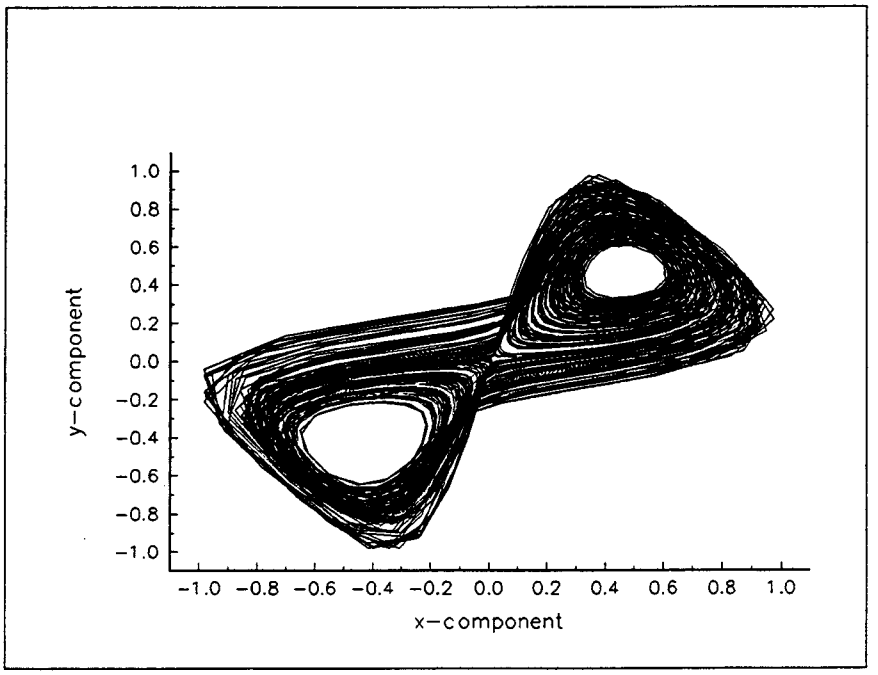

Fig. 10. The attractor reconstructed by using delay coordinates of the iterated map. Five thousand points are shown.

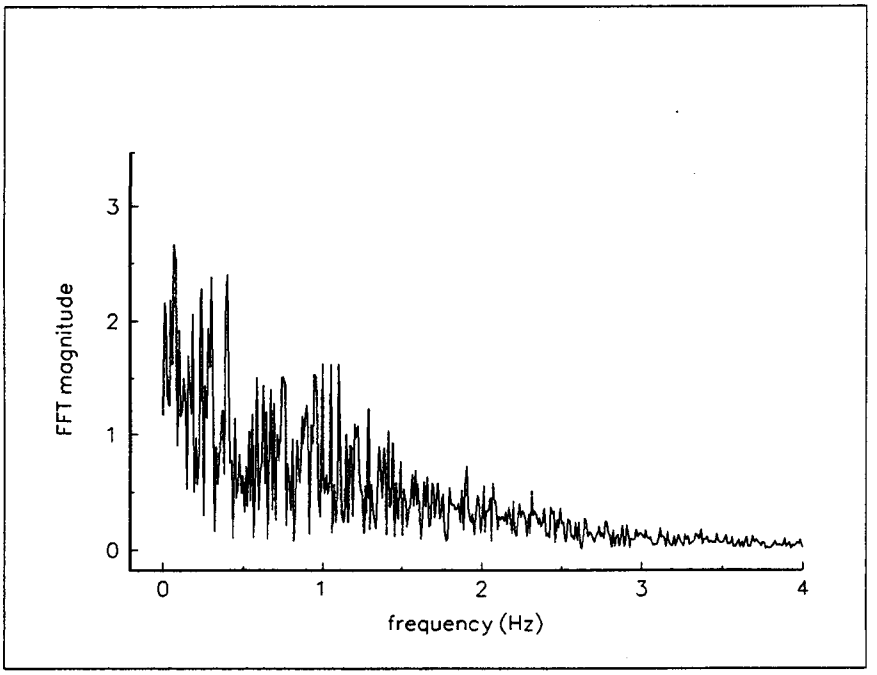

Fig. 11. The Fourier transform of the Lorenz time series.

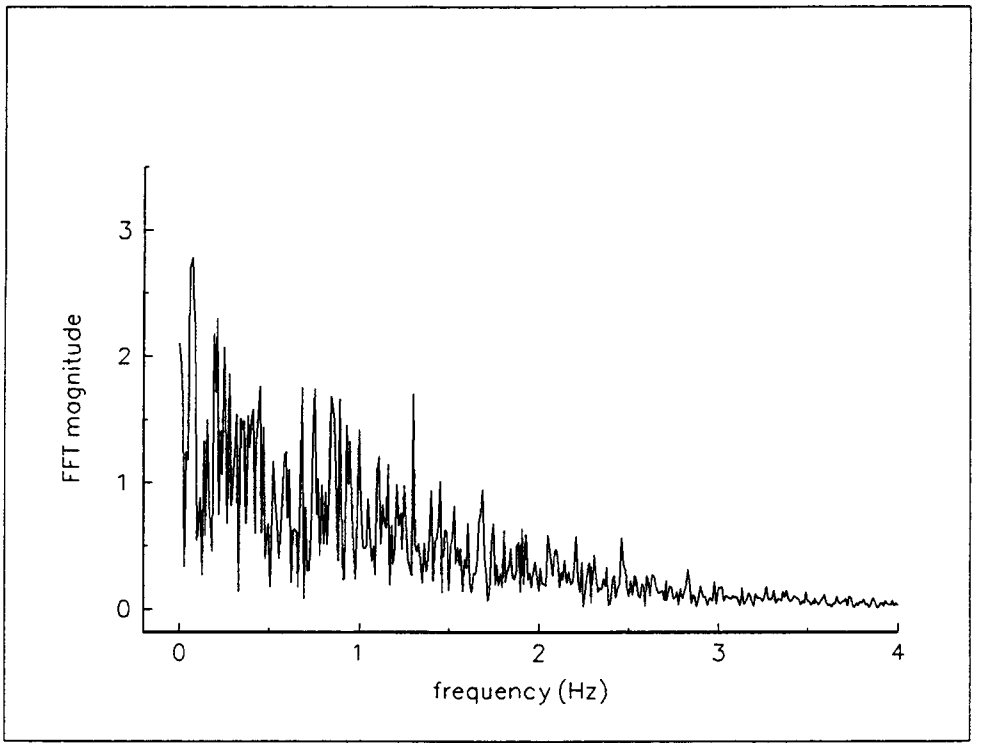

Fig. 12. The Fourier transform of the time series generated by iterating the map of the Lorenz attractor.

2.4 CONCLUSIONS

Overall, polynomial maps have proven unsatisfactory for use in signal masking. The unconstrained polynomial maps perform well as one-step predictors, but their tendency to approach a fixed point or to become unbounded under iteration makes them unsuitable for generating a masking signal. Constrained polynomial maps are poor one-step predictors, and, while they remain bounded and do not approach a fixed point under iteration, they do not closely approximate the dynamics of the original system. These maps could be used to generate a masking signal, but that signal would be unlike the measured data used to calculate the map coefficients.

The RBF maps have shown a remarkable ability to simulate the dynamics of the three systems examined in this work. In each of the three cases, the time series, attractors, and Fourier transforms of the original and simulated time series compare well. The RBF maps do not approach either infinity or a fixed point for any number of iterations. Although the number of terms in the maps (i.e., hundreds) may seem excessive, the coefficient calculation is performed on the Silicon Graphics Indy workstation in a matter of several minutes, and the map iteration is performed in approximately 10 seconds. Thus, the RBF maps appear to be computationally practical.

Experience has shown that the ability of the RBF maps to approximate the time series depends heavily on N (N also corresponds to the amount of data used to fit the values of the λ_n), on the value of β, on the value of C, and on the selection of the basis vectors. Although the effects of these parameters on map performance has not been fully explored, our preliminary work indicates the following:

- The map will approximate richer, more complicated behavior as more terms are added. It is speculated that this behavior is caused by the relatively limited dynamics used in the fit for a small number of terms. For a successful approximation of the system dynamics, it appears that the number of terms in the fit must correspond to the number of points required to adequately display the system dynamics.

- The map will be more robust for small (in an absolute sense) values of β. For larger values of β, the maps have a greater tendency to approach a fixed point under iteration. A value of $\beta = 1$ has given good results in our work.

- The value of C affects the amplitude of the iterated map. As C approaches the maximum value of the data, the amplitude of the iterated map approaches that of the data. Values of C much larger or smaller than the maximum data value result in the amplitude of the iterated map being less than that of the data. In this work, good results were obtained for values of C between 50% and 100% of the maximum data value.

- The basis vector selection is critical to the map performance. In this work, the coordinates of the first N points were used as the basis vectors. Other methods of selection, such as

choosing every 10th point or selecting some arbitrary set of basis vectors, produced poorer results.

Although the effects of β, C, d_e, N, and the selection of the basis vectors on map performance are not fully understood, some "rules of thumb" have been developed that have resulted in maps that qualitatively reproduce the dynamics of the original systems. Further work should concentrate on developing a better understanding of the effects of these parameters on map performance, ultimately leading to more rigorous methods for selecting these parameters.

3. MAP PERFORMANCE USING MEASURED TIME SERIES

Hydrophone data were acquired from Exuma Sound, Bahamas, through the generosity of the Naval Surface Warfare Center, Carderock Division (CDNSWC). An RBF map was created to model the dynamics that generated these data. This section describes the map creation and compares performance of the map with the measured time series.

3.1 MAPPING OF EXUMA SOUND TIME SERIES

Hydrophone data were collected in Exuma Sound by personnel aboard the USNS Hayes in May 1996. The data were collected from a single hydrophone at a depth of 400 ft in calm conditions. The data sampling rate was 4096 samples/second, and the data was low pass filtered, with a cutoff frequency of approximately 1600 Hz. Approximately 3 minutes of data were obtained. Because the Exuma Sound time series was measured and not generated from a set of nonlinear differential equations, the embedding dimension was not known in advance. Thus, the additional step of determining the embedding dimension is required when creating a map to simulate the data measured at Exuma Sound.

The first step in the time series analysis is to determine the optimum time delay to use in reconstructing the attractor. The mutual information for the Exuma Sound time series is shown in Fig. 13. The first minimum in the mutual information occurs for a time delay of approximately 0.003 seconds, so this time delay is used to reconstruct the attractor.

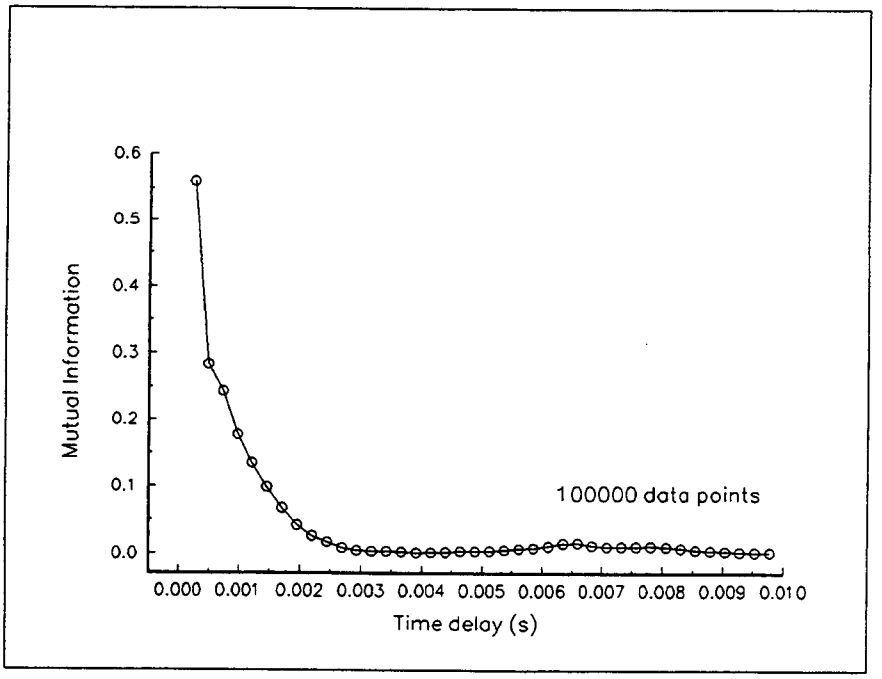

Fig. 13. The mutual information for a range of time delays for the Exuma Sound data.

Figure 14 shows the global false nearest neighbor calculation results for the Exuma Sound time series. The calculation was performed for 400,000 data points with a set of 100 selected points, and for 600,000 data points with sets of 300 or 1000 selected points. Figure 14 shows a minimum of approximately 20% in the percentage of false nearest neighbors for an embedding dimension of eight; the percentage of false nearest neighbors increases rapidly for embedding dimensions greater than eight. Using larger data sets and larger sets of selected points reduces the rate of increase in the percentage of false nearest neighbors for embedding dimensions greater than d_e. This results occurs because more "true" nearest neighbors are found for larger data sets and because the effects of a few poor nearest neighbor selections are reduced for larger sets of selected points. These results indicate that d_e equals eight and that the data are heavily contaminated with random noise.

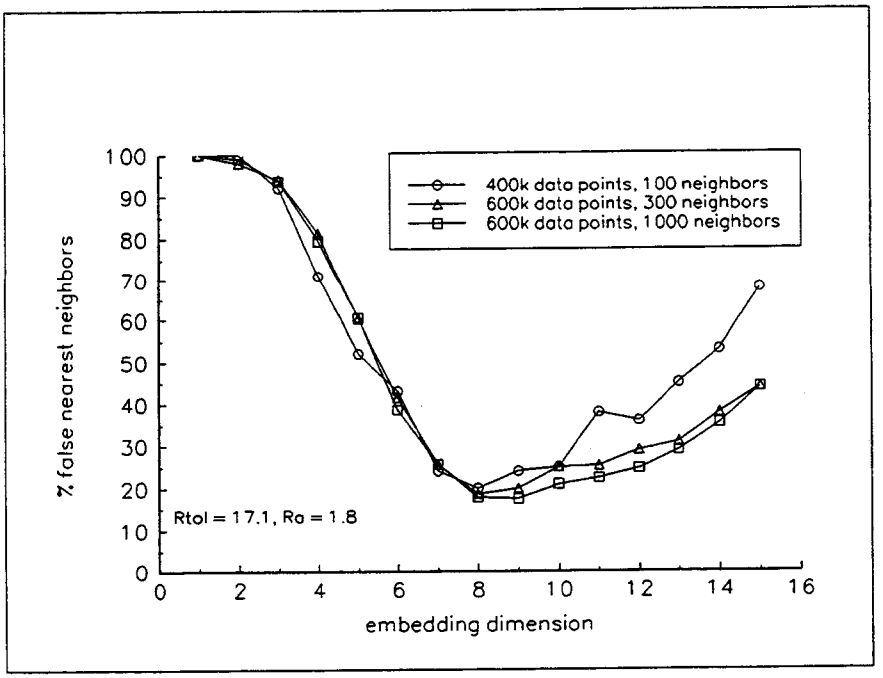

Fig. 14. Percentage of false nearest neighbors calculated by using the Exuma Sound data.

A 600-term RBF map was created using values of $\beta = 1$ and $C = 1$ and an embedding dimension of eight. The original and simulated time series and Fourier transforms are compared in Figs. 15 to 18. The qualitative behavior of the two time series is similar, as shown by the close agreement between the original and simulated time series and Fourier transforms.

The RBF map has performed well in simulating the dynamics of the Exuma Sound data. This example shows that the mapping technique using radial basis functions is robust in the sense that it is able to produce good results for both the "clean" data of the Lorenz system of Section 3 and the noisy data measured at Exuma Sound. This robustness is encouraging and indicates that the method may successfully applied to other data sets.

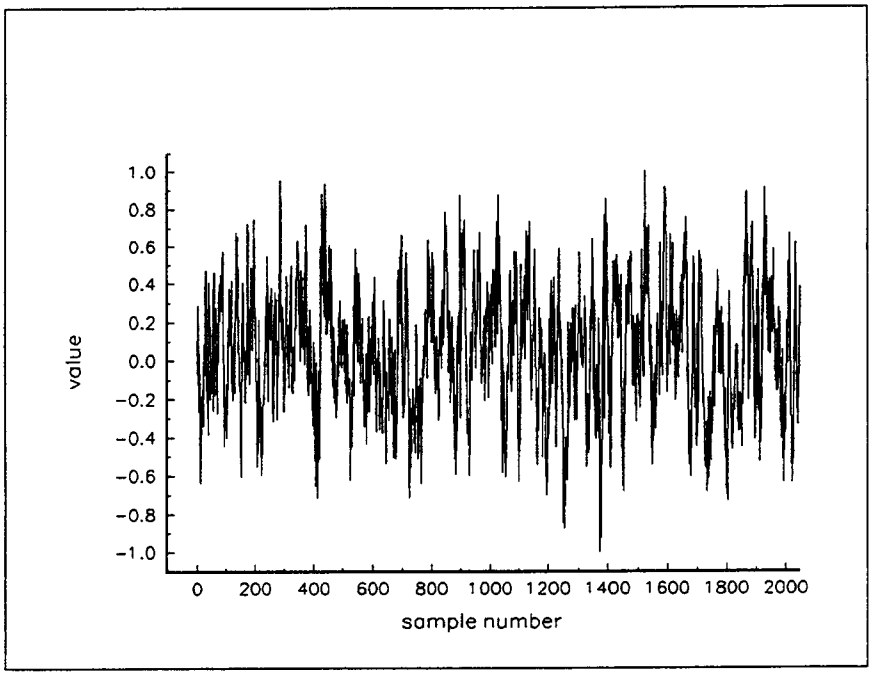

Fig. 15. The measured time series from the Exuma Sound data. The sample rate is 4096 samples/second.

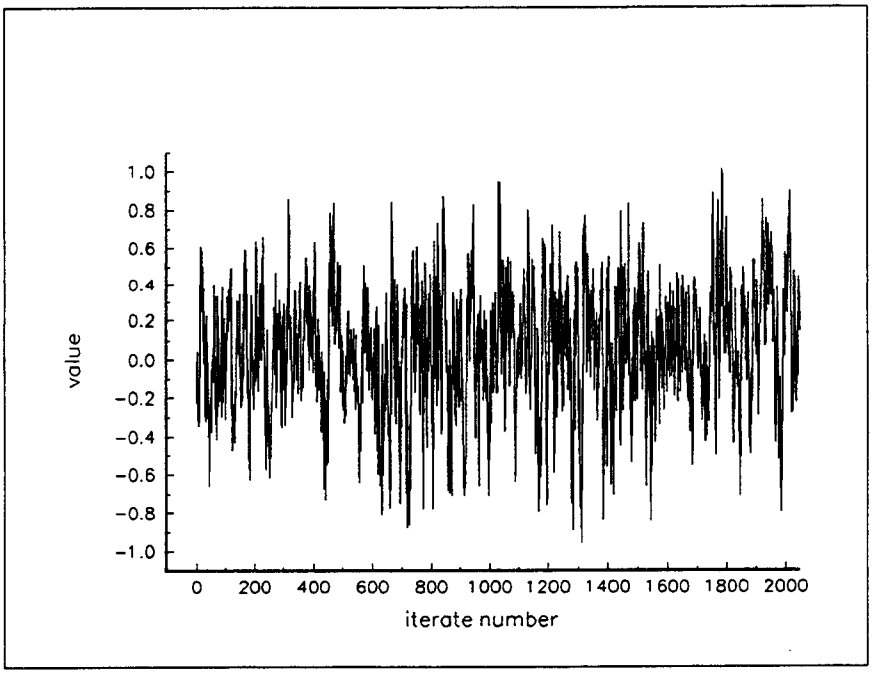

Fig. 16. The time series generated from iterating the map. The map has 600 terms and is composed of radial basis functions with $\beta = 1$ and $C = 1$. Eight dimensions are used in the reconstruction with a time delay of 0.0030 seconds.

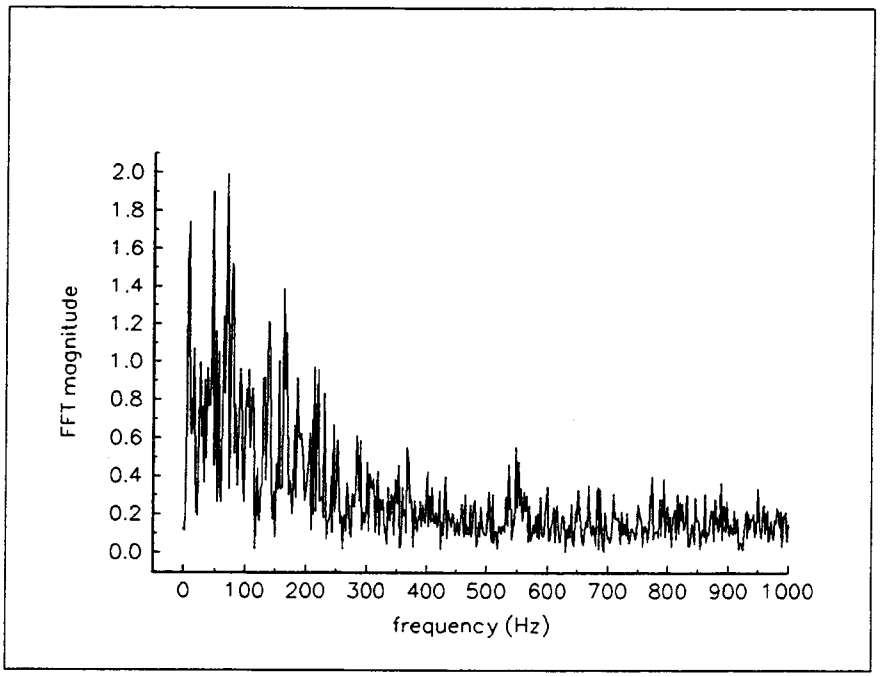

Fig. 17. The Fourier transform of the Exuma Sound time series.

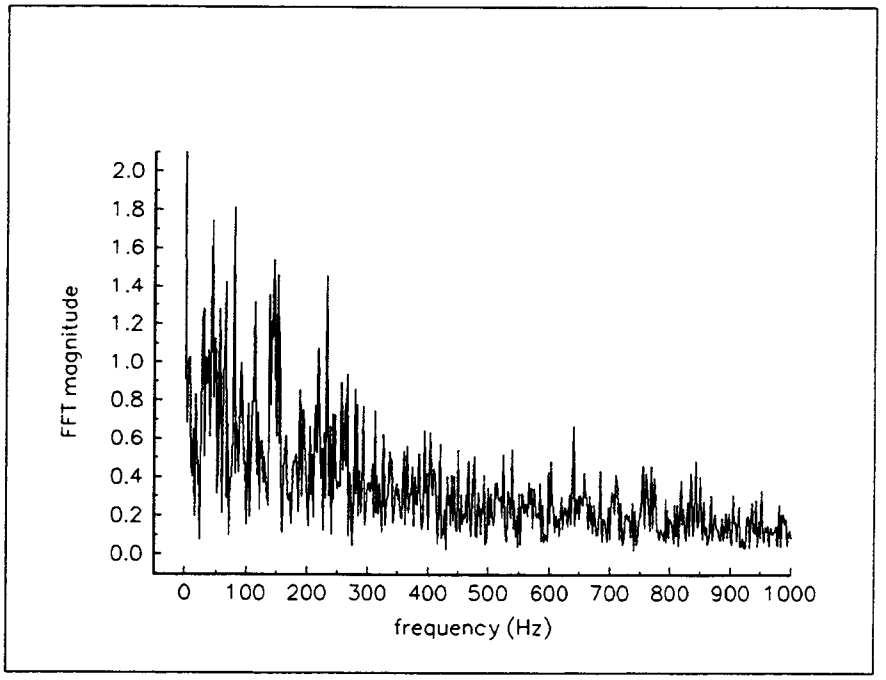

Fig. 18. The Fourier transform of the time series generated by iterating the map of the Exuma Sound time series.

4. SIGNAL MASKING METHODOLOGY

Demodulation of the received signal requires that the masking signal be available at the receiver. An approach for reconstructing the masking signal at the receiver is to use a masking signal possessing the property of self-synchronization.[13,14] Such systems can be divided into a drive system and one or more stable response subsystems (i.e., subsystems with only negative Liapunov exponents).[13] When driven, the output from the stable response subsystems will converge to the values of the drive system.[13] Moreover, this synchronization can, for some systems, be robust in the sense that the output from the stable response systems is not particularly sensitive to small deviations in the drive signal. Thus, for such systems, the transmitted signal can be used as the drive signal, and the response of the stable response subsystems can be used to closely approximate the masking signal.

This concept has been applied to signal masking by using both the Lorenz system and Chua's circuit.[14,15] These systems are described by nonlinear systems of differential equations that exhibit the property of self-synchronization and are robust with respect to noise. In each case, the ability to send and receive a masked signal, recover the masking signal at the receiver, and then demodulate the received signal to recover the encrypted information with acceptable accuracy was demonstrated.

This approach, while elegant, has the major drawback that the noise profile used to generate the masking signal (such as the Exuma Sound data) may not be generated by a system that will synchronize. Furthermore, it was not clear what constraints needed to be placed on the maps to guarantee synchronization. Therefore, another technique was sought that either forced synchronization of the maps at the transmitter and receiver or made synchronization unnecessary. This section describes a simple signal masking and recovery scheme that performs satisfactorily.

4.1 SIGNAL MASKING AND RECOVERY SCHEME

A simple definition of synchronization between two dynamical systems is that given a subset of the state variables of the first system as input, the state variables of the second system will converge to those of the first system. Thus, the transmission of some state variables generated by a driving system allows the remaining state variables to be reproduced by a driven system at the receiver. The resulting state variables are then used to reproduce the masking signal, which can be used to extract the information from the received signal.

Using the method of delays to reconstruct the state variables inherently removes the issue of synchronization. One variable is measured, and the remaining state variables are obtained from delayed versions of this measured variable. Thus, the only remaining question is how best to mask the information. A very simple scheme was used in this investigation to include the information signal with the masking signal. The information signal was added to every other sample of the masking signal, and the time delay used in the method of delays was adjusted to correspond to an even number of samples. The resulting transmitted signal, which was created by simply adding the information signal to the masking signal, could then be demodulated by

subtracting the predicted signal from the received signal. Because the information was added only to every other sample, and because the sample increment corresponding to the state vector reconstruction was even, the masking signal corresponding to a sample with added information was predicted using measured signal values that did not contain added information. Thus, the predicted masking signal at the receiver (assuming no noise or signal corruption) exactly equals the masking signal at the transmitter. The masked information can be recovered nearly exactly.

4.2 SIGNAL MASKING AND RECOVERY USING THE LORENZ SYSTEM

Signal masking and recovery is demonstrated in this section using the Lorenz attractor as the dynamical system. The 400-term RBF map described in Sect. 2.3.2.1 was used to mask and demask a sine wave. The sine wave amplitude was 1% of the peak-to-peak amplitude of the masking signal, had a frequency was 0.1 Hz, and was added to the masking signal beginning with the 600th sample. Figures 19 and 20 show the Fourier transform of the masking signal and the masking signal with the added sine wave. It is unlikely that any difference between these two signals would be noticed. Figure 21 shows the recovered signal; the recovered signal which is virtually identical to the information added to the masking signal.

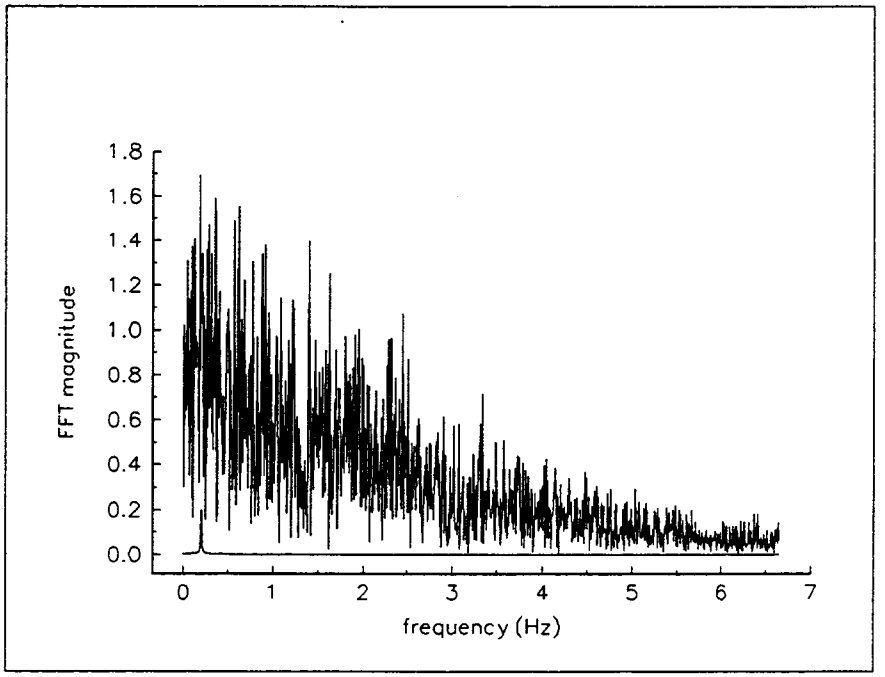

Fig. 19. The Fourier transform of the masking signal combined with the sine wave. The masked sine wave is also shown.

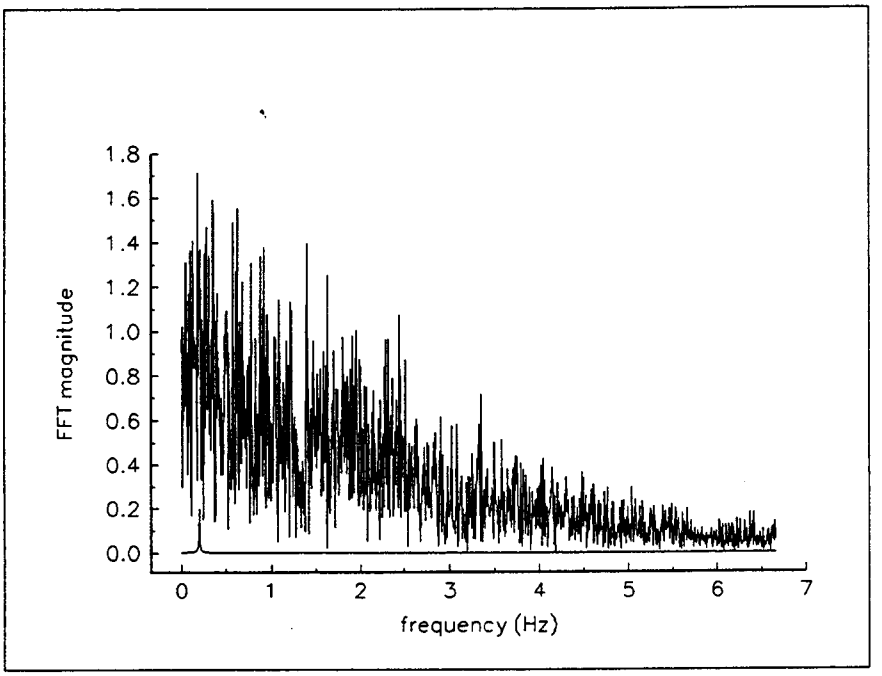

Fig. 20. The Fourier transform of the masking signal (the time series formed by iterating the map of the Lorenz attractor). The masked sine wave is also shown.

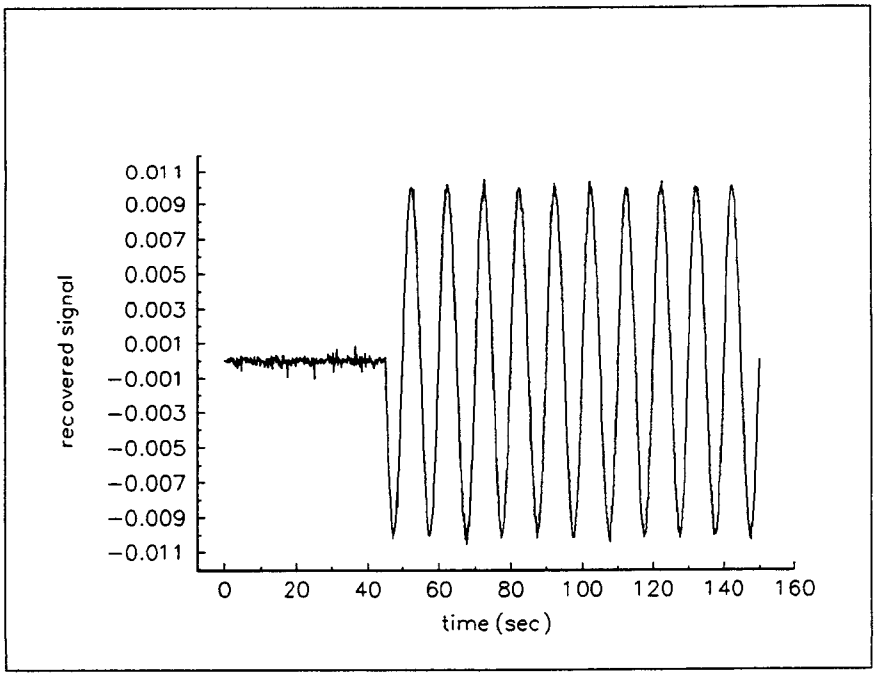

Fig. 21. The recovered sine wave.

4.3 SIGNAL MASKING AND RECOVERY USING THE EXUMA SOUND DATA

The Exuma Sound data were also used to demonstrate signal masking and recovery. The 600-term RBF map described in Sect. 3.1 was used to create the masking signal. The sine wave amplitude was 1% of the peak-to-peak amplitude of the masking signal, had a frequency was 0.1 Hz, and was added to the masking signal beginning with the 600th sample. Figures 22 and 23 show the Fourier transform of the masking signal and the masking signal with the added sine wave. Again, it is unlikely that any difference caused by the inclusion of the sine wave would be noticed. Figure 24 shows the recovered signal; again, the recovered signal is virtually identical to the information added to the masking signal.

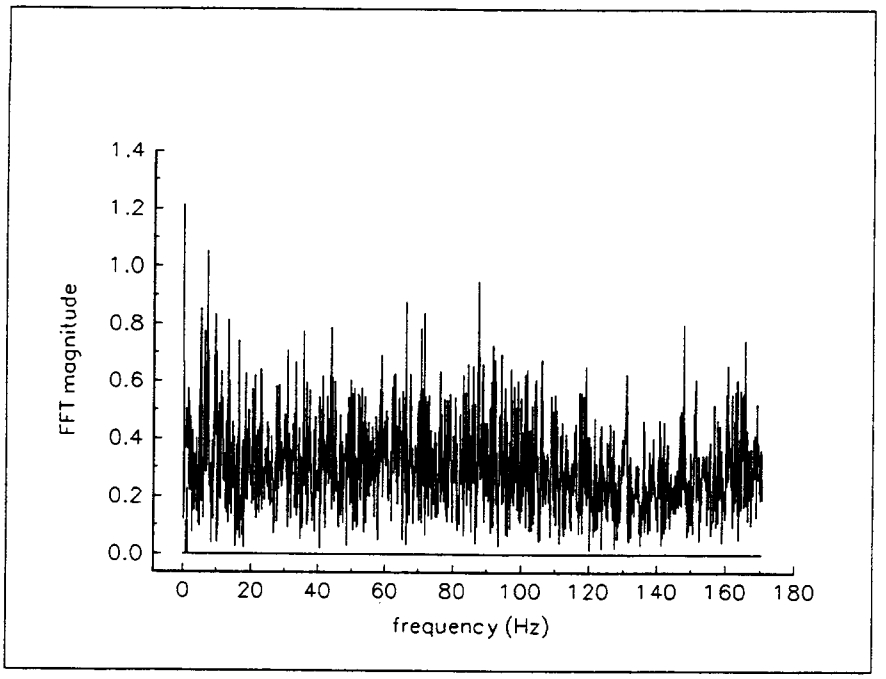

Fig. 22. The Fourier transform of the masking signal (the time series formed by iterating the map of the Exuma Sound time series).

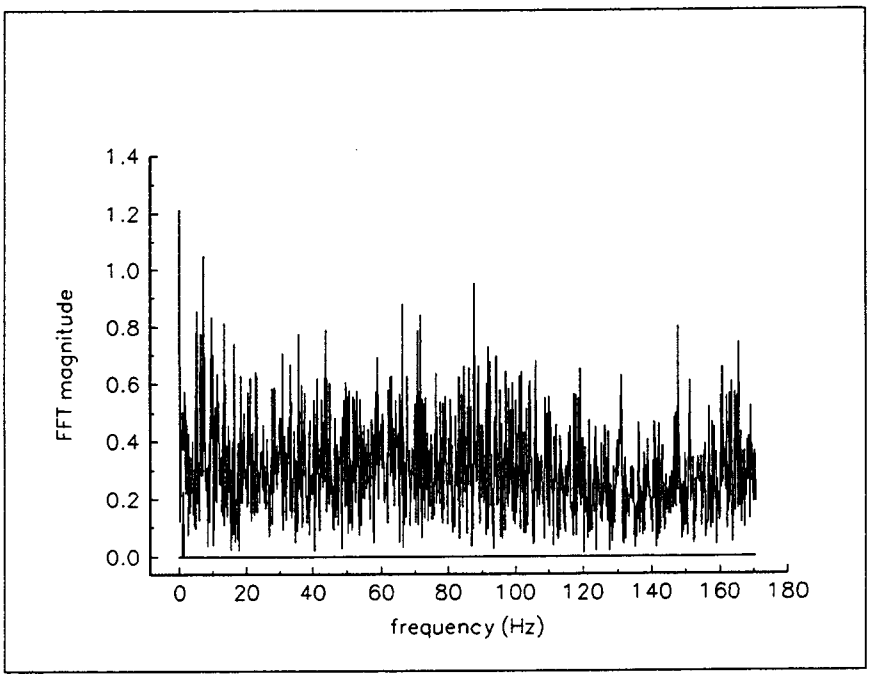

Fig. 23. The Fourier transform of the masking signal combined with the sine wave.

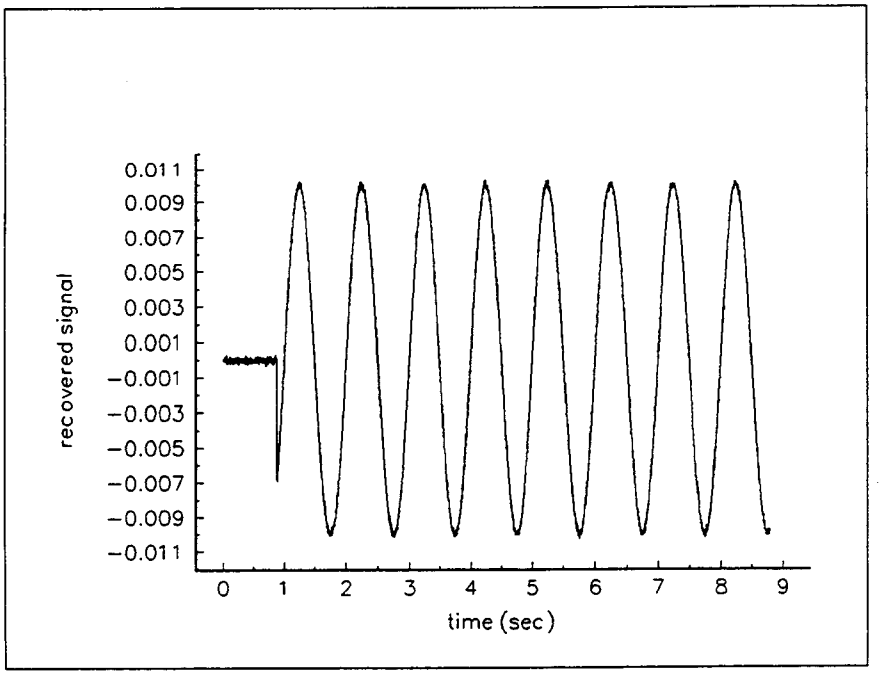

Fig. 24. The recovered signal.

5. PERFORMANCE OF SIGNAL MASKING AND RECOVERY IN A PHYSICAL MEDIUM

All previous results reported here regarding this method have come from computer simulations. Performance of the signal masking/recovery method in a physical medium is presented in this section. The effect of the transmission channel on the received signal must be taken into account when performing a masked transmission. A simple way to account for the effects of the transmission channel is to use different maps at the transmitter and the receiver. The transmitter map is created first and is used to form a time series. This time series is then transmitted and received, forming a new time series at the receiver that includes the effects of the transmission channel. A receiver map is then created using the received time series. This receiver map is then used during signal recovery to predict the values of the masking signal at the receiver. The masking signal is then removed from the received signal, leaving a distorted version of the masked information.

5.1 MASKING AND RECOVERY USING THE LORENZ SYSTEM

The Lorenz system was again used to demonstrate the masking method. The line-in/line-out ports of a Silicon Graphics Indy workstation provided a low-noise, high-fidelity transmission path.

A 6-dimensional, 400-term RBF map was used as the transmitting map. The time series produced by iterating this map was transmitted and received through the line-in/line-out ports for a Silicon Graphics Indy workstation. The received time series was used to create a receiving map, which also was 6 dimensional and contained 400 terms. A transmission that included a masked 2-Hz sine wave with an amplitude of 20% of the masking signal maximum value was transmitted and received. The received signal was demasked by using the receiving map. A comparison of the original sine wave and the recovered sine wave is shown in Fig. 25 (the sine wave is coarsely represented because the sampling rate is only 6.7 Hz). Close examination shows that the main features of the sine wave are recovered at the receiver.

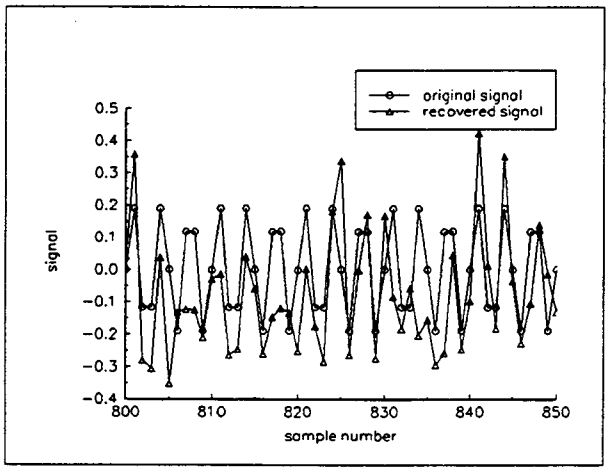

Fig. 25. Time domain comparison of the original and recovered 2-Hz sine wave.

Figure 26 shows a frequency domain comparison of the original sine wave and the recovered sine wave. The recovered signal is attenuated by a factor of 0.7 during transmission, reception, and recovery. Noise created during transmission and reception is clearly evident in both the time and the frequency domain comparisons. This noise is at a relatively low level and has not severely impacted the ability of the method to recover the masked sine wave.

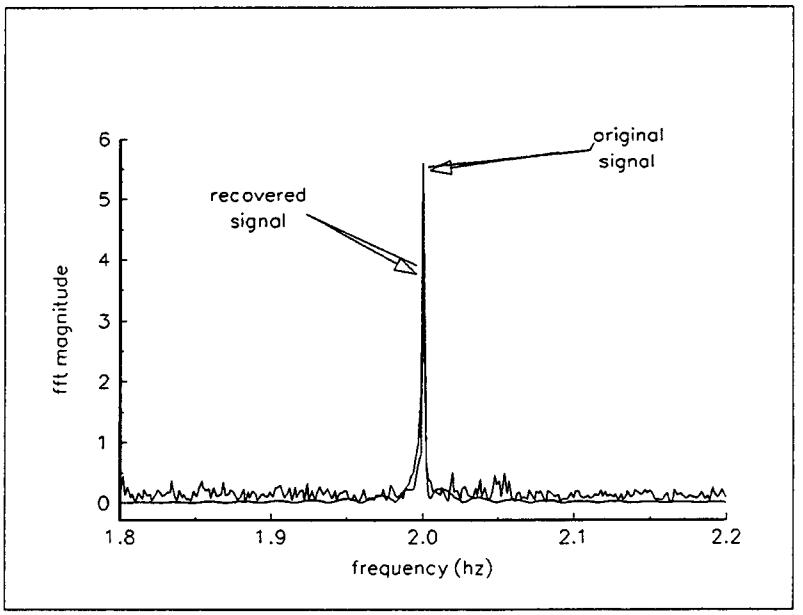

Fig. 26. Frequency domain comparison of the original and recovered 2-Hz sine wave.

5.2 MASKING AND RECOVERY USING THE EXUMA SOUND DATA

The Exuma Sound data were also used to demonstrate the masking method. The line-in/line-out ports of the Silicon Graphics Indy workstation again provided a low-noise, high-fidelity transmission path. A 9-dimensional, 400-term RBF map was used as the transmitting map for the Exuma Sound data. The time series resulting from iterating this map was transmitted and received by using the line-in/line-out ports of the Silicon Graphics Indy workstation. The received time series was used to create a receiving map, which also was 14 dimensional and contained 800 terms. The additional dimensions and terms were used in an attempt to increase the accuracy of the map to function as a one-step predictor. A transmission that included a masked 10 Hz sine wave with an amplitude of 20% of the masking signal maximum value was transmitted and received. The received signal was demasked by using the receiving map. Figure 27 compares the original sine wave and the recovered sine wave. The sine wave is clearly shown as a low-frequency modulation of the noisy signal.

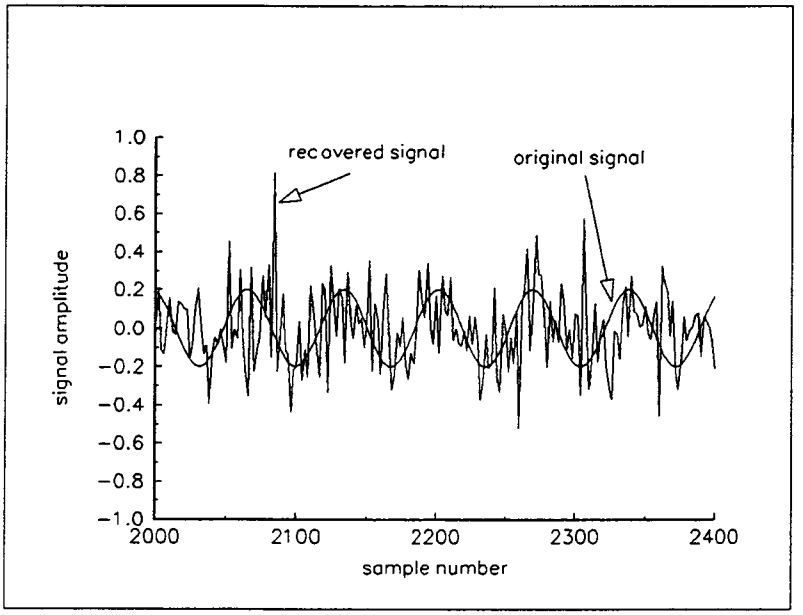

Fig. 27. Time domain comparison of the original and recovered 10-Hz sine wave.

A frequency domain comparison of the original sine wave and the recovered sine wave is shown in Fig. 28. The recovered signal is attenuated by a factor of approximately 0.4 during transmission, reception, and recovery. Again, noise created during transmission and reception is clearly evident in both the time and the frequency domain comparisons. This noise is at a somewhat higher level than that experienced with the Lorenz system during a similar transmission and accounts for the additional attenuation of the recovered signal. This level of noise does not prevent the masked sine wave from being recovered.

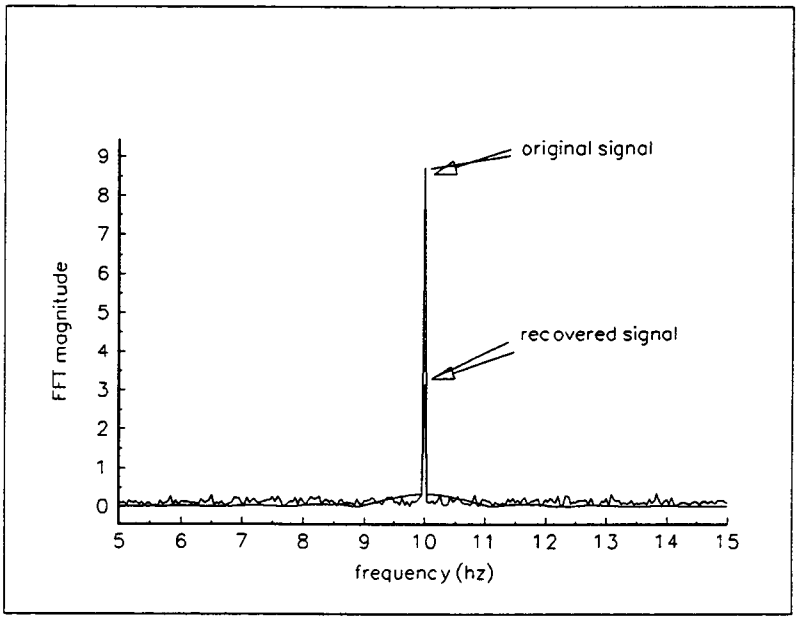

Fig. 28. Frequency domain comparison of the original and recovered 10-Hz sine wave.

6. SUMMARY AND CONCLUSIONS

This investigation of masking methodology has resulted in significant progress toward the creation of a practical method for masking information signals by using a masking signal that closely approximates ambient noise. This section reviews the most significant accomplishments of the investigation and discusses the areas in which additional research efforts are needed.

6.1 RESEARCH ACCOMPLISHMENTS

A method for creating maps that closely approximate a measured noise signal in both time and frequency domains has been developed and demonstrated. The method of delays was used to reconstruct the multidimensional trajectory of the measured time series. The time corresponding to the first minimum in the mutual information function of the time series was used as the optimum time delay. The method of global false nearest neighbors was used to determine the optimum embedding dimension of the trajectory. This information was then used to reconstruct the trajectory of ambient ocean noise.

After reconstructing the trajectory, expansions in polynomials and RBF were used to create maps for predicting the next point in the time series given sufficient previously measured points. The map coefficients were calculated by using the method of least squares to fit the map predictions to the measured data. We found that both polynomial maps and RBF maps could accurately predict the next time series value, given previously measured values for non-noisy data, but that polynomial maps would typically converge to a limit cycle or a fixed point under iteration. RBF maps performed better than polynomial maps under iteration, usually producing a time series that closely approximated the original time series used to create the map.

We concluded that RBF maps would be useful for creating maps for masking data, because these maps produced time series that closely approximate the original time series and usually do not converge to limit cycles or fixed points. Both polynomial and RBF maps could be used to recover a masked signal.

We devised a method for adding information to the masking signal that allowed the masking signal to be accurately reproduced at the receiver (assuming no transmission path noise or distortion). Because the method of delays allows a representation of a trajectory to be created from the measurement of a single variable, the trajectory of the received signal can be reconstructed in the same way it was reconstructed at the transmitter. Thus, if the map used to create the masking signal is available at the receiver, the masking signal can be accurately reproduced. Forcing the delay time used to reconstruct the trajectory to correspond to an even number of samples and adding the information to every other sample of the masking signal forces the prediction of every other masking signal sample (which corresponds to samples that contain information) to be made with samples that do not contain any masked information. Thus, predictions of the masking signal samples corresponding to transmitted signals containing information are very accurate (again, assuming no noise or signal distortion), and the information can be recovered. The effectiveness of this simple method has been demonstrated in both

computer simulations and limited laboratory experiments, and it has been shown that this approach avoids the need to synchronize the maps at the transmitter and receiver.

Another simple but effective method was devised to take the effects of the transmission path into account when recovering the information at the receiver. If transmission were perfect, the same map used at the transmitter could be used to reproduce the masking signal at the receiver. Because of signal distortion during transmission, this approach will not result in an accurate version of the masking signal being produced at the receiver. If the masking signal without noise is transmitted and received, the received signal, which is simply a distorted version of the masking signal, can be used to create a polynomial or RBF map that can predict the next measured value given previous values. This map can then be used at the receiver to produce the received masking signal, assuming the same time delay is used to reconstruct the trajectory at the receiver. The resulting recovered signal is a distorted version of the original information, with the distortion resulting from the transmission path.

Signal masking/demasking was demonstrated by using both simulated signals and measured noise (i.e., background) signals. We used RBFs to create maps that produced time series that closely approximated the trajectories of the Lorenz system and measured hydrophone data from Exuma Sound. These maps were used to mask information by simply adding a sine wave to the map's time series. Computer simulations of the transmission and reception of the masked signals showed that the masking signal could be reproduced at the receiver and that the masked information could be accurately recovered. Transmission through a low-noise, high-fidelity transmission path introduced distortion into the recovered signal, but the information was still recovered. Transmission through a high-noise, low-fidelity transmission path resulted in no useful information being recovered. Thus, it was shown that the method in its present form requires a low-noise, high-fidelity transmission path or some digital form of transmission that will very accurately reproduce the original masked signal. Nevertheless, it was demonstrated that information can be masked in a synthetic time series that appears like some form of measured noise and that this information can be transmitted, received, and recovered using this technique.

6.2 AREAS FOR FUTURE RESEARCH

The limited investigation described in this report was able to only touch on some important issues regarding the use of maps to simulate measured time series and to mask information. This section discusses some of the issues that need to be more adequately understood to fully develop the signal masking method.

Map stability is still not well understood (here stability is defined as maps that will not approach a fixed point or a limit cycle under iteration). Although some work has been performed to determine constraints that will guarantee stability, this work is far from complete. RBF maps appear to never approach a fixed point and rarely fall into a limit cycle. However, these possibilities cannot be completely dismissed, so the issue of stability needs to be more thoroughly addressed before the method can be claimed to be completely practical.

Concerted efforts should be made to reduce the sensitivity of the maps to noise. The maps used in this work generally consist of hundreds of terms and attempt to mimic the dynamics of nonlinear systems. It is not surprising that a small amount of noise added to each of the map terms causes a large change in a map's output. Some work performed as part of this investigation indicates that RBF maps will become less sensitive to noise as the number of centers is reduced. However, our experience has shown that the ability of a map to act as an accurate one-step predictor is generally enhanced by increasing the number of centers. A method to select the optimum number of centers and their coordinates is needed to create maps that optimize some combination of noise sensitivity and prediction accuracy.

The optimum data processing that needs to be performed on the measured signals is still unclear. The data is normalized and shifted to have mean zero, but the optimum scaling has not been determined. Our work has shown that map performance is highly dependent on the proper scaling of the data and that the scaling of the measured data, both at the transmitter and at the receiver, is critical to the method's performance.

The form of the information signal and how it can best be included with the masking signal has not been investigated in this work. The simple addition of the two signals performed in this work is clearly not the most secure way to hide the information in the masking signal, but it was a good choice for the purpose of investigating the masking method feasibility. Some form of encryption of the information by using spread spectrum techniques should be considered, or possibly modulation of map coefficients would result in a well-hidden signal. Undoubtably, a large number of ways exist to include the information with the masking signal, and a more thorough investigation of these should be performed.

6.3 CONCLUSIONS

This investigation has shown it is possible to create maps by applying tools originally developed to analyze nonlinear systems, that closely approximate the behavior of complex dynamic systems such as chaotic systems or measured noise. These maps are stable in the sense that they approach neither a limit cycle nor a fixed point under iteration and will function as an accurate one-step predictor.

A simple method based on the inherent properties of trajectory reconstruction by using the method of delays and involving proper selection of reconstruction time delay and proper inclusion of information with the masking signal ensures that in the absence of noise and distortion, the masking signal can be accurately reconstructed at the receiver. This simple method avoids the complicated issue of synchronization that must be addressed when using other masking methods in which the masking signal is generated from sets of differential equations.

This investigation provided another simple method to address the issue of signal distortion caused by the transmission path. Two maps are used. The first map is created from a time series of the background noise and is used as the masking signal at the transmitter. The second map is created by using a received version of the masking signal. This second map will account for the

effects of the transmission path. This simple method allows for the effects of the transmission path to be accounted for during signal recovery without having to perform a complicated and time-consuming dynamic analysis of the transmission path.

The signal masking method was demonstrated by using a computer simulation of a transmission (i.e., a perfect transmission/reception); a transmission through a low-noise, high-fidelity transmission path; and a transmission through a high-noise, low-fidelity transmission path. The computer simulation of the transmission showed the method to perform extremely well, with the information signal being recovered almost perfectly. The transmission through the low-noise, high-fidelity transmission path showed that the information could still be recovered, but the information was distorted and noisy. The information could not be recovered when the transmission occurred through the high-noise, low-fidelity transmission path.

It can be concluded that the sensitivity to noise of the method in its present form limits its use in applications involving low-noise, high-fidelity, transmissions. It may be possible to apply the method to radio frequency transmissions, but it is unlikely it could be successfully applied to the field that originally motivated this work—sonar and undersea communications. The method could be used with little modification to hide information on recorded media, especially in digital form, or on printed media, such as in the form of hidden watermarks. Other specific applications may come to light with time.

7. REFERENCES

1. H. Leung, and T. Lo, "Chaotic Radar Signal Processing over the Sea," *IEEE Journal of Ocean Engineering*, **18 (3), 287—95 (July 1993)**.

2. H. Leung, "Applying Chaos to Radar Detection in an Ocean Environment: An Experimental Study," *IEEE Journal of Ocean Engineering*, **20 (1), 56–64 (January 1995)**.

3. J. R. Puchler, T. Serre, Z. Kollath, and J. Mattei, "A Chaotic Pulsating Star – The Case of R Scuti," *Physical Review Letters*, **74, 842–45 (1995)**.

4. T. Serre, Z. Kollath, and J. R. Buchler, "Search for Low Dimensional Chaos in Variable Stars, The Global Polynomial Phase-Space Reconstruction Method," *Astronomy and Astrophysics*, 15.2 (1995).

5. N. H. Packard, J. P. Crutchfield, J. D. Farmer, and R. S. Shaw, "Geometry From a Time Series", *Physical Review Letters*, **45, 712 (1980)**.

6. F. Takens, "Detecting Strange Attractors in Turbulence," pp. 366–81 in *Dynamical Systems and Turbulence, Warwick 1980*, ed. D. A. Rand and L. S. Young, *Lecture Notes in Mathematics* **898** Berlin (1981).

7. M. Fraser, and H. L. Swinney, *Independent Coordinates for Strange Attractors from Mutual Information*, Physical Review A, **33 (2) 1134–40 (February 1986)**.

8. M. B. Kennel, R. Brown, and H. D. I. Abarbanel, *Determining Embedding Dimension for Phase-Space Reconstruction Using a Geometrical Construction*, Physical Review A, **45 (6), 3403–11 (March 1992)**.

9. H. G. Schuster, *Deterministic Chaos: An Introduction*, Weinheim, Federal Republic of Germany (1988).

10. R. Brown, P. Bryant, and H. D. I. Abarbanel, *Computing the Lyapunov Spectrum of a Dynamical System from an Observed Time Series*, Physical Review A, **43 (6) 2787–2806 (March 1991)**.

11. M. Giona, F. Lentini, and V. Cimagalli, *Functional Reconstruction and Local Predication of Chaotic Time Series*, Physical Review A, **44 (6) (September 1991)**.

12. M. Casdagli, *Nonlinear Prediction of Chaotic Time Series*, Physica D, **35, 335–56 (1989)**.

13. L. M. Pecora and T. L. Carroll, "Synchronization in Chaotic Systems," *Physical Review Letters*, **64 (8) 821–24 (February 1990)**.

14. K. M. Cuomo, and A. V. Oppenheim, "Robustness and Signal Recovery in a Synchronized Chaotic System," *International Journal of Bifurcation and Chaos*, **3 (6), 1629–38 (1993)**.

15. C. W. Wu, and L. O. Chua, "A Simple Way To Synchronize Chaotic Systems With Applications to Secure Communication Systems," *International Journal of Bifurcation and Chaos*, **3 (6), 1619–27 (1993)**.

INTERNAL DISTRIBUTION

1. G. T. Alley
2-11. J. E. Breeding
12. N. E. Clapp, Jr.
13-22. B. Damiano
23. W. B. Dress, Jr.
24. R. G. Gilliland
25. R. A. Hess
26. S. W. Kercel
27. J. M. Jansen, Jr.
28. D. W. McDonald
29. G. N. Miller
30. T. P. Sjoreen
31. J. O. Stiegler
32. R. W. Tucker, Jr.
33. J. D. White
34. Central Research Library
35. Y-12 Technical Reference Section
36. Laboratory Records—Record Copy
37. I&C Division Publications Office
38. ORNL Patent Section

EXTERNAL DISTRIBUTION

39. Ron Moore, The RM Group, Inc., 12024 Broadwood Drive, Knoxville, TN 37922
40. David Norton, Houston Advanced Research Center, 4800 Research Forest Drive, The Woodlands, TX 77381
41. M. M. Sevik, Carderock Division, Naval Surface Warfare Center, Code 70, Bethesda, MD 20084-5000
42. Ernesto Suarez, Pratt & Whitney, P.O. Box 109600, Mail Stop 716-87, West Palm Beach, FL 33410-9600
43-44. Office of Scientific and Technical Information, U.S. Department of Energy, P.O. Box 62, Oak Ridge, TN 37831